Spatial–Spectral Multiscale Sparse Unmixing for Hyperspectral Images

Taner Ince, Nicolas Dobigeon

▶ **To cite this version:**

Taner Ince, Nicolas Dobigeon. Spatial–Spectral Multiscale Sparse Unmixing for Hyperspectral Images. IEEE Geoscience and Remote Sensing Letters, 2023, 20, pp.1-5. 10.1109/LGRS.2023.3328370 . hal-04280429

HAL Id: hal-04280429
https://hal.science/hal-04280429

Submitted on 11 Nov 2023

HAL is a multi-disciplinary open access archive for the deposit and dissemination of scientific research documents, whether they are published or not. The documents may come from teaching and research institutions in France or abroad, or from public or private research centers.

L'archive ouverte pluridisciplinaire **HAL**, est destinée au dépôt et à la diffusion de documents scientifiques de niveau recherche, publiés ou non, émanant des établissements d'enseignement et de recherche français ou étrangers, des laboratoires publics ou privés.

Spatial-Spectral Multiscale Sparse Unmixing for Hyperspectral Images

Taner Ince, *Member, IEEE*, Nicolas Dobigeon, *Senior Member, IEEE*

***Abstract*—We propose a simple yet efficient sparse unmixing method for hyperspectral images. It exploits the spatial and spectral properties of hyperspectral images by designing a new regularization informed by multiscale analysis. The proposed approach consists of two steps. First, a sparse unmixing is conducted on a coarse hyperspectral image resulting from a spatial smoothing of the original data. The estimated coarse abundance map is subsequently used to design two weighting terms summarizing the spatial and spectral properties of the image. They are combined to define a sparse regularization embedded into a unmixing problem associated with the original hyperspectral image at full resolution. The performance of the proposed method is assessed with numerous experiments conducted on synthetic and real data sets. It is shown to compete favorably with state-of-the-art methods from the literature with lower computational complexity.**

***Index Terms*—Sparse unmixing, spatial regularization, total variation, reweighting.**

I. Introduction

REMOTE Earth sensing based on infrared hyperspectral sensors embedded on aerial vehicles or satellite is referred to as hyperspectral imaging (HSI). Since it delivers images of high spectral resolution, it has been used in many areas such as agriculture, defence industry, and mineral exploration. One of the main problem when analyzing hyperspectral image is their limited spatial resolution. Thus a hyperspectral pixel may be associated with a large area of the Earth surface. Since these areas are not expected to be composed of a single material, the measured spectra often consist of a mixture of several elementary signatures associated with pure. Spectral unmixing aims at decomposing the mixed pixels into pure signatures (endmembers) and corresponding proportions (abundances). Most of the unmixing algorithms assume a linear mixture model (LMM), i.e., the observed spectra are linear combinations of the endmember signatures, weighted by the corresponding abundances. Basically, a spectral unmixing pipeline first identifies the endmembers and then the corresponding abundances are estimated by a dedicated inversion algorithm. Pixel purity index (PPI) [1], N-FINDR [2] and vertex component analysis (VCA) [3] are popular endmember extraction algorithms which assume that there is at least one pixel representative of each sought endmember signature. Besides, since the endmember and abundance matrices are expected to be nonnegative, numerous unmixing algorithms have also elaborated on the nonnegative matrix factorization paradigm [4] (see, e.g., [5]–[11]).

When the endmember signatures are assumed to belong to a given possibly large spectral library, recovering the abundance maps is generally formulated as a sparse regression problem. Efficient algorithms to solve the resulting problems are the variants of the sparse unmixing by variable splitting and augmented Lagrangian (SUnSAL) framework [12]. Several improvements of SUnSAL have been proposed in the literature to better exploit the expected spectral or spatial properties of the hyperspectral data [13]–[16]. For instance, collaborative SUnSAL (C-SUnSAL) implicitly exploits the spectral redundancy between measured pixel spectra by enforcing the joint sparsity of the abundance matrix. On the other hand, SUnSAL-TV includes total variation (TV) in the original objective function to promote a piece-wise spatial content [14].

Although TV based unmixing comes with good unmixing performance, its complexity results in high computational times. To lighten this computational burden, so-called multiscale unmixing algorithms (MUA) have been designed to replace the TV regularization by relevant surrogates easier to embed into an optimization scheme. These approaches consist in solving two simple sparse regression problems defined in two domains of distinct spatial resolutions [17]. The first one is solved in an approximation domain resulting from a segmentation step and provides a low-resolution abundance map. This map is used to design a spatial regularization which is subsequently embedded into the second problem formulated in the full resolution domain. Thanks to its simplicity, MUA has a much lower computational complexity than TV based approaches but it may be shown to smooth edges [17]. Recently, fast sparse unmixing (FastUn) builds on this multiscale approach while simultaneously preserving crisp edge details thanks to a spatial discontinuity strategy [18].

Another line of work consists in designing regularizations that jointly capture the spatial content and the spectral redundancy inherent to hyperspectral data. For instance, double reweighted sparse regression and TV (DRSU-TV) overcomes the high mutual correlation between spectral signatures by exploiting the spatial-spectral properties in a single regularizer with a reweighting strategy [15]. Spectral-spatial weighted sparse unmixing (S^2WSU) enhances the sparsity of the solution thanks to a double reweighting term in a single regularizer

Part of this work has been supported by the ANR-3IA Artificial and Natural Intelligence Toulouse Institute (ANITI) under grant agreement ANITI ANR-19-PI3A-0004 and by the ANR IMAGIN project under grant agreement ANR-21-CE29-0007.

Taner Ince is with the Department of Electrical and Electronics Engineering, Gaziantep University, 27310 Gaziantep, Turkey (e-mail:tanerince@gantep.edu.tr).

Nicolas Dobigeon is with the University of Toulouse, IRIT/INP-ENSEEIHT, 31000 Toulouse, France, and also with the Institut Universitaire de France (IUF), France (e-mail: nicolas.dobigeon@enseeiht.fr).

Corresponding author: Taner Ince

governed by a unique parameter [16]. Other works extract the spatial and spectral information by using superpixel segmentation strategies. Superpixel-based reweighted low-rank and total variation (SUSRLR-TV) promotes low-rank abundance maps in each superpixel with a complementary TV regularization [19]. Superpixel based graph Laplacian for sparse unmixing (SBGLSU) minimizes the differences in each superpixel using a graph Laplacian summarizing the spatial-spectral content [20]. Double spatial graph Laplacian regularization for sparse unmixing (DSGLSU) employs a transformation in each superpixel to produce coarse abundances [21]. They are subsequently used in a weighting term when recovering the full resolution abundance maps, granted with a graph Laplacian-based regularization in each superpixel. However, these later works remain computational demanding because of the use of a graph Laplacian.

Combining the advantages brought by the two families of unmixing methods mentioned above, this paper proposes a so-called spatial-spectral multiscale sparse unmixing (S^2MSU) method. Following a multiscale approach, it consists in solving two sparse unmixing problems defined at two different scales. The first one is formulated in a coarse domain, where the approximated data is obtained by a sliding window strategy which extracts the spatial-spectral properties of the hyperspectral data. The second one is formulated in the full resolution domain where the low-resolution abundance map estimated in the first step is used to derive a spatial-spectral regularization. The computational complexity of the method is significantly lower than those of competitive algorithms without sacrificing the unmixing accuracy. Even though the recently proposed FastUn algorithm [18] shares some similarities with the proposed S^2MSU method, it is worth noting that the former does not exploit the spectral redundancy inherent to the hyperspectral data. Contrary to the proposed S^2MSU method, the design of the FastUn regularization is only motivated by spatially motivated arguments.

The paper is organized as follows. The proposed method is described in Section II. Section III provides experimental results obtained on simulated and real data sets. Section IV concludes the paper.

II. Spatial-spectral multiscale sparse unmixing (S^2MSU)

Like most unmixing methods from the literature, the proposed approach builds on the LMM, i.e., neglecting multiple scattering effects. This model states that each pixel spectrum results from the linear combination of endmember signatures whose contributions are weighted by the abundances. More precisely, let $\mathbf{Y} = [\mathbf{y}_1, \ldots, \mathbf{y}_n] \in \mathbb{R}^{L\times n}$ denote the matrix whose columns are the L-band spectra measured in the n pixels. According to LMM, this matrix can be modeled as

$$\mathbf{Y} = \mathbf{A}\mathbf{X} + \mathbf{N} \tag{1}$$

where $\mathbf{A} \in \mathbb{R}^{L\times m}$ and $\mathbf{X} \in \mathbb{R}^{m\times n}$ are the endmember and abundance matrices, respectively and $\mathbf{N} \in \mathbb{R}^{L\times n}$ accounts for any mismodeling and observation noise. This work frames the unmixing task into a supervised context, i.e., the endmember matrix is assumed to be known as a (possibly) large spectral library composed of endmember candidates. In such a context, unmixing the hyperspectral image boils down to estimating the abundance matrix $\mathbf{A}$. This task is generally formulated as a sparse regression problem [22]. The proposed S^2MSU algorithm elaborates on this formulation by designing a simple yet sound regularization. Similarly to the multiscale approaches, it consists in solving two subproblems defined at two distinct spatial resolutions. First, essential spatial and spectral information is extracted by unmixing a low-resolution counterpart of the original image. Then the recovered low-resolution abundance map is used to regularize a sparse unmixing problem formulated in the original full resolution domain. These steps are detailed in what follows.

A. Extracting the spatial and spectral information

In a first step of the proposed S^2MSU algorithm, a low-resolution version of the original image is generated by applying an averaging filter chosen as square window with fixed size. The spatially smooth image is denoted as $\bar{\mathbf{Y}} = [\bar{\mathbf{y}}_1, \ldots, \bar{\mathbf{y}}_{\bar{n}}] \in \mathbb{R}^{L\times\bar{n}}$ whose ith column is given by

$$\bar{\mathbf{y}}_i = \frac{1}{|\mathcal{P}_i|}\sum_{l\in\mathcal{P}_i}\mathbf{y}_l. \tag{2}$$

where $\mathcal{P}_i$ represents the set of pixel indices in the window centered in the ith pixel and $|\mathcal{P}_i|$ is the window size (with $\bar{n} \ll n$). A low-resolution abundance map $\bar{\mathbf{X}}$ can be obtained by solving the sparse unmixing problem

$$\min_{\bar{\mathbf{X}}} \frac{1}{2}\|\bar{\mathbf{Y}} - \mathbf{A}\bar{\mathbf{X}}\|_{\mathrm{F}}^2 + \bar{\lambda}\|\mathbf{W}\odot\bar{\mathbf{X}}\|_1 + \iota_+(\bar{\mathbf{X}}) \tag{3}$$

where $\bar{\lambda}$ is regularization parameter and $\iota_+(\cdot)$ is the indicator function ensuring the nonnegative constraint. The solution of (3) can be efficiently approximated by using a splitting trick after introducing auxiliary variables. The resulting algorithmic scheme is summarized in Algo. 1, where ϵ is a small value to prevent numerical instabilities and the maximum $\max(\cdot)$, the soft-thresholding $\mathrm{soft}(t,\delta) = \mathrm{sign}(t)\max\{|t|-\delta, 0\}$ and the inversion $\cdot^{-1}$ should be understood as component-wise operators. Besides, it is worth noting that the matrix $\mathbf{W}$ is adjusted along the iterations to enhance the sparsity of the solution, following a standard iterative re-weighting strategy (see Steps 4 and 5 in Algo. 1).

B. Including the spatial and spectral information

Since $\bar{\mathbf{X}}$ is expected to capture the spatial and spectral properties of the image, it is subsequently used to design two weighting matrices defining a data-informed regularization. First, a coarse abundance map $\mathbf{S} = [\mathbf{s}_1, \ldots, \mathbf{s}_n] \in \mathbb{R}^{m\times n}$ at full resolution is obtained using a piece-wise constant interpolation[1]

$$\forall i \in \{1, \ldots, \bar{n}\},\ \forall j \in \mathcal{P}_i,\ \mathbf{s}_j = \bar{\mathbf{x}}_i. \tag{4}$$

[1]Shared pixels should be averaged in case of the use of overlapping sliding windows.

Algorithm 1 1st subproblem: low-resolution unmixing.

Input: $\bar{\mathbf{Y}}$, $\mathbf{A}$, $\bar{\lambda}$, $\mu > 0$, ϵ,
Initialization: $k = 0$, $\mathbf{V}_1^{(0)}$, $\mathbf{V}_2^{(0)}$, $\mathbf{D}_1^{(0)}$, $\mathbf{D}_2^{(0)}$
$\mathbf{\Lambda} = \mathbf{A}^T\mathbf{A} + 2\mu\mathbf{I}$
while not converged **do**
  $\mathbf{X}^{(k+1)} = \mathbf{\Lambda}^{-1}(\mathbf{A}^T\bar{\mathbf{Y}} + \mu(\mathbf{V}_1^{(k)} + \mathbf{V}_2^{(k)} + \mathbf{D}_1^{(k)} + \mathbf{D}_2^{(k)}))$
  $\mathbf{w}_i = \frac{1}{\|(\mathbf{X}^{(k+1)} - \mathbf{D}_1^{(k)})_{i,:}\|_2 + \epsilon} \quad i = 1, \ldots, m$
  $\mathbf{W}_{:,i} = [\mathbf{w}_1, \ldots, \mathbf{w}_m]^T \quad i = 1, \ldots, \bar{n}$
  $\mathbf{V}_1^{(k+1)} = \text{soft}(\mathbf{X}^{(k+1)} - \mathbf{D}_1^{(k)}, (\bar{\lambda}/\mu)\mathbf{W})$
  $\mathbf{V}_2^{(k+1)} = \max(\mathbf{0}, \mathbf{X}^{(k+1)} - \mathbf{D}_2^{(k)})$
  $\mathbf{D}_1^{(k+1)} = \mathbf{D}_1^{(k)} - (\mathbf{X}^{(k+1)} - \mathbf{V}_1^{(k+1)})$
  $\mathbf{D}_2^{(k+1)} = \mathbf{D}_2^{(k)} - (\mathbf{X}^{(k+1)} - \mathbf{V}_2^{(k+1)})$
  $k \leftarrow k + 1$
end while
Output: $\bar{\mathbf{X}} = \mathbf{X}^{(k)}$

Then, this low-resolution abundance map is used to defined the two weighting matrices

$$\mathbf{W}_1 = \text{diag}\left(\left[\frac{1}{\|\mathbf{S}_{1,:}\| + \epsilon}, \ldots, \frac{1}{\|\mathbf{S}_{m,:}\| + \epsilon}\right]\right) \quad (5)$$

$$[\mathbf{W}_2]_{ij} = \frac{1}{s_{ij} + \epsilon} \quad (6)$$

The full-resolution abundance map is finally estimated by solving

$$\min_{\mathbf{X}} \frac{1}{2}\|\mathbf{Y} - \mathbf{A}\mathbf{X}\|_{\text{F}}^2 + \lambda\|\mathbf{W}_1\mathbf{W}_2 \odot \mathbf{X}\|_1 + \iota_+(\mathbf{X}) \quad (7)$$

where the matrix product $\mathbf{W}_1\mathbf{W}_2$ acts as a weighting term. This formulation has the great advantage of combining both spectral and spatial information in the form of a single regularizer. First, akin to collaborative unmixing, the matrix $\mathbf{W}_1$ enforces a group sparsity of the abundance matrix. It penalizes the abundance coefficients in the row associated with endmembers that have been identified as hardly present over the whole set of pixels. Indeed only a few materials in the endmember matrix $\mathbf{A}$ is expected to contribute jointly to the mixtures. Second, the matrix $\mathbf{W}_2$ penalizes the abundance associated with neighboring pixels in the same way. It can be interpreted as a surrogate of the conventional TV. Solving (7) can be achieved with the same strategy as for the problem (3), summarized by Algo. 2. It is worth noting that the weighting term $\mathbf{W}_1\mathbf{W}_2$ is now constant along the iterations, which ensures the algorithm convergence more easily.

The computational complexity of S^{2}MSU is driven by Algo. 1 and Algo. 2. Algo. 1 solves the unmixing problem in a low resolution domain following an optimization scheme similar to SUnSAL [12]. Algo. 2 adopts the same strategy to solve the unmixing problem in the full resolution domain, after precomputing the weighting matrices $\mathbf{W}_1$ and $\mathbf{W}_2$. Since $\bar{n} \ll n$, Algo. 2 dominates the computational complexity of S^{2}MSU, which is of the order of $\mathcal{O}(nmL)$ per iteration.

Algorithm 2 2nd subproblem: full-resolution unmixing.

Input: $\mathbf{Y}$, $\mathbf{A}$, $\mathbf{W}_1$,$\mathbf{W}_2$, λ, $\mu > 0$, ϵ
Initialization: $k = 0$, $\mathbf{V}_1^{(0)}$, $\mathbf{V}_2^{(0)}$, $\mathbf{D}_1^{(0)}$, $\mathbf{D}_2^{(0)}$
$\mathbf{\Lambda} = \mathbf{A}^T\mathbf{A} + 2\mu\mathbf{I}$
while not converged **do**
  $\mathbf{X}^{(k+1)} = \mathbf{\Lambda}^{-1}(\mathbf{A}^T\mathbf{Y} + \mu(\mathbf{V}_1^{(k)} + \mathbf{V}_2^{(k)} + \mathbf{D}_1^{(k)} + \mathbf{D}_2^{(k)}))$
  $\mathbf{V}_1^{(k+1)} = \text{soft}(\mathbf{X}^{(k+1)} - \check{\mathbf{X}} - \mathbf{D}_1^{(k)}, (\lambda/\mu)\mathbf{W}_1\mathbf{W}_2)$
  $\mathbf{V}_2^{(k+1)} = \max(\mathbf{0}, \mathbf{X}^{(k+1)} - \mathbf{D}_2^{(k)})$
  $\mathbf{D}_1^{(k+1)} = \mathbf{D}_1^{(k)} - (\mathbf{X}^{(k+1)} - \check{\mathbf{X}} - \mathbf{V}_1^{(k+1)})$
  $\mathbf{D}_2^{(k+1)} = \mathbf{D}_2^{(k)} - (\mathbf{X}^{(k+1)} - \mathbf{V}_2^{(k+1)})$
  $k \leftarrow k + 1$
end while
Output: $\hat{\mathbf{X}} = \mathbf{X}^{(k)}$

III. Experimental results

The proposed S^{2}MSU algorithm[2] is compared to several sparse unmixing from the literature: SUnSAL [12], SUnSAL-TV [14], S^{2}WSU [16], DRSU-TV [15], MUA [17], FastUn [18] and SUSRLR-TV [19]. Their performance is assessed by computing the signal reconstruction error (SRE) defined as $\text{SRE} = 10\log_{10}\frac{\|\mathbf{X}\|_{\text{F}}^2}{\|\mathbf{X} - \hat{\mathbf{X}}\|_{\text{F}}^2}$ where $\mathbf{X}$ and $\hat{\mathbf{X}}$ are the reference and estimated abundance matrices, respectively. Moreover, the behavior of sparse unmixing algorithms is frequently monitored by evaluating the sparsity degree of the recovered abundance maps. Thus, the algorithms are also compared with respect to the smooth sparsity measure $\rho = \text{numel}(\hat{\mathbf{X}} \geq 5 \times 10^{-3})/\text{numel}(\hat{\mathbf{X}})$ where $\text{numel}(\cdot)$ count the number of elements.

A. Simulated data sets

Two hyperspectral images of sizes 100×100 pixels, referred to as SD1 and SD2, are simulated according to LMM (1). The corresponding abundance maps are generated to mimic plausible spatial material distributions, as depicted in Fig. 1 for two particular endmembers. SD1 is mostly composed of crisp regions and homogeneous regions while SD2 is mostly composed of homogeneous regions. A spectral library $\mathbf{A}$ is created by selecting $m = 240$ signatures from the spectral library splib06 [23] with $L = 224$ spectral bands ranging from 0.4 to 2.5μm. The two images SD1 and SD2 are generated by selecting 9 active signatures from $\mathbf{A}$ and adding Gaussian noises with different signal-to-noise ratios (SNR): SNR$\in \{20\text{dB}, 30\text{dB}, 40\text{dB}\}$. All algorithms are run using their optimal parameters as prescribed in their original papers. The window and step size for the proposed S^{2}MSU algorithm are selected as 10 and 5, respectively. This choice obeys a certain bias-variance trade-off. Indeed too small windows do not capture the key spatial structures and are expected to be more sensitive to noise or outliers. Conversely too large windows tend to smooth small details.

SRE and ρ values obtained by the compared algorithms are reported in Table I. The proposed method S^{2}MSU is shown to reach the best SRE and sparsity levels for SNR$\in \{20\text{dB}, 30\text{dB}\}$. This good performance obtained in the high

[2]The code is available at https://ndobigeon.github.io/soft/demo_S2MSU.rar.

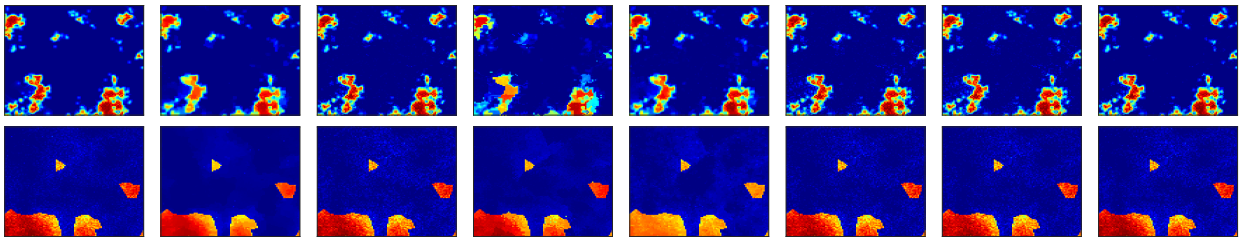

Fig. 1. Estimated abundance maps for endmember #1 in SD1 (top) and endmember #9 in SD2 (bottom) with SNR= 30dB.

TABLE I
SIMULATED DATA SETS: SRE AND SPARSITY LEVELS OBTAINED BY THE COMPARED ALGORITHMS.

			SUnSAL TV	S²WSU	DRSU TV	MUA	FastUn	SUSLR TV	S²MSU
SD1	20dB	SRE	6.23	6.35	6.82	6.45	12.19	7.54	**13.38**
		ρ	0.0899	0.0382	0.0480	0.0752	0.0229	0.0652	**0.0122**
	30dB	SRE	11.12	20.73	13.80	8.15	19.55	11.91	**21.85**
		ρ	0.0500	0.0187	0.0281	0.0664	0.0174	0.0325	**0.0125**
	40dB	SRE	17.32	**30.95**	17.96	11.43	28.47	21.12	30.41
		ρ	0.0413	0.0136	0.0179	0.0568	0.0152	0.0170	**0.0122**
SD2	20dB	SRE	11.81	6.92	13.75	14.13	16.25	15.21	**17.38**
		ρ	0.0723	0.0351	0.0418	0.0583	0.0233	0.0510	**0.0126**
	30dB	SRE	17.87	21.22	13.55	18.15	20.70	21.03	**21.76**
		ρ	0.0433	0.0230	0.0362	0.0492	0.0223	0.0332	**0.0190**
	40dB	SRE	20.79	**27.43**	13.77	19.34	27.24	24.89	27.22
		ρ	0.0515	0.0251	0.0314	0.0486	0.0260	0.0316	**0.0245**

TABLE II
JASPER RIDGE DATA SET: SRE AND SPARSITY LEVELS OBTAINED BY THE COMPARED ALGORITHMS.

	SUnSAL TV	S²WSU	DRSU TV	MUA	FastUn	SUSLR TV	S²MSU
SRE	8.42	14.00	10.67	9.37	**15.16**	9.09	14.87
ρ	0.0163	0.0051	0.0087	0.0184	0.0051	0.020	**0.0050**

TABLE III
SIMULATED AND REAL DATA SETS: COMPUTATIONAL TIMES REQUIRED BY THE COMPARED ALGORITHMS.

	SUnSAL TV	S²WSU	DRSU TV	MUA	FastUn	SUSLR TV	S²MSU
SD1	103	37	161	**5**	11	173	14
SD2	102	36	160	**4**	10	188	11
Cuprite	1200	373	1293	**116**	132	2094	152
Jasper Ridge	215	72	231	82	**29**	425	58

noise scenarios can be explained by the contribution of the proposed regularization. Informed by the low-resolution abundance maps estimated in the 1st stage of the algorithm, the weighting matrix acts as an averaging filter to mitigate the noise. For SNR = 40dB, S^{2}MSU provides competitive results.

These conclusions can also be validated with visual inspections. Fig. 1 shows the reference and estimated abundances for SNR =30dB. In particular, the maps recovered by S^{2}MSU seem to better preserve the homogeneous regions as well as the crisp details, contrary to SUnSAL-TV and DRSU-TV.

B. Real data sets

Two real data sets are used to validate the efficiency of S^{2}MSU. In a first experiment, a 250×191-pixel portion of the Cuprite data set[3] is extracted. This portion includes most of the active minerals in the region. The original data includes 224 bands but some water absorption and noisy bands have been removed prior to analysis. The spectral library $\mathbf{A}$ is chosen as a collection of $m = 498$ spectral signatures from the splib06 library. Since this data set is not accompanied by a ground truth in terms of abundance maps, the results are evaluated qualitatively by visual comparison with the classification map provided by Tetracorder 4.4 [24]. Fig. 2 shows the estimated abundance maps obtained by the compared algorithms for chalcedony mineral. The algorithms S^{2}WSU, FastUn and S^{2}MSU seem to better preserve the details, contrary to TV-based methods.

A second experiment is performed on the Jasper Ridge data set[4]. The considered region-of-interest is composed of 100×100 pixels with $L = 198$ spectral bands after removing bad bands. The endmember matrix $\mathbf{A}$ is made of 498 spectral signatures from the splib06 complemented by 4 endmembers provided with data set, namely tree, water, soil and dirt ($m = 502$). Since ground truth abundance maps are also provided with this data set, Table II reports the SRE and ρ values for all compard algorithms. These results show that FastUn and S^{2}MSU reach the best results. This can also be assessed by visual inspection in Fig. 3.

The computation times required by the compared algorithms are reported in Table III. MUA has the lighter computational burden while FastUn and S^{2}MSU behave similarly.

IV. CONCLUSION

This paper proposes a two step sparse unmixing adopting a multiscale approach. The 1st step consists in performing a conventional sparse unmixing in a domain of low spatial resolution. This domain is defined by degrading the resolution of the original hyperspectral data. The estimate low resolution abundance map is used to design two weighting terms which are combined to form a spatial-spectral regularization. Embedded into a sparse unmixing problem formulated in the original full resolution domain, this regularization jointly acts as a surrogate of group sparsity and data-informed spatial smoothing. Thanks to their simplicity, the two optimization problems can be efficiently solved thanks to variable splitting

[3]Available at http://aviris.jpl.nasa.gov/html/aviris.freedata.html.

[4]Available at https://rslab.ut.ac.ir/data.

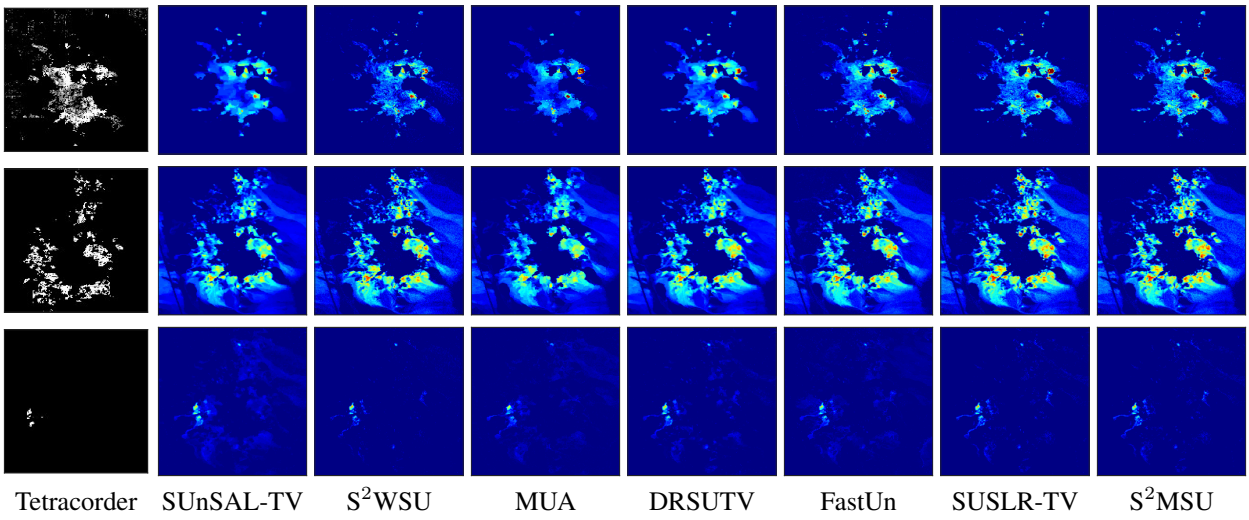

Fig. 2. Cuprite data set: abundance maps estimated by the compared algorithms (top to bottom: chalcedony, alunite and buddingtone).

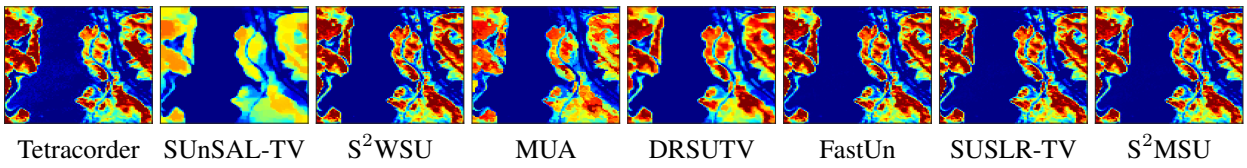

Fig. 3. Jasper Ridge data set: abundance maps for the tree endmember estimated by the compared algorithms.

strategy. The algorithm is shown to provide satisfactory unmixing performance when compared to state-of-the-art algorithms from the literature, as assessed by extensive experiments conducted on two synthetic and two real data sets.

REFERENCES

[1] J. W. Boardman, F. A. Kruse, and R. O. Green, "Mapping target signatures via partial unmixing of AVIRIS data," in *Fifth JPL Airborne Earth Science Workshop*, vol. 95. JPL Publication, 1995, pp. 23–26.

[2] M. E. Winter, "N-findr: An algorithm for fast autonomous spectral endmember determination in hyperspectral data," in *Imaging Spectrometry V*, vol. 3753. International Society for Optics and Photonics, 1999, pp. 266–275.

[3] J. M. P. Nascimento and J. M. B. Dias, "Vertex component analysis: a fast algorithm to unmix hyperspectral data," *IEEE Trans. Geosci. Remote Sens.*, vol. 43, no. 4, pp. 898–910, April 2005.

[4] D. D. Lee and H. S. Seung, "Learning the parts of objects by non-negative matrix factorization," *Nature*, vol. 401, no. 6755, pp. 788–791, 1999.

[5] S. Jia and Y. Qian, "Constrained nonnegative matrix factorization for hyperspectral unmixing," *IEEE Trans. Geosci. Remote Sens.*, vol. 47, no. 1, pp. 161–173, Jan 2009.

[6] X. Wang, Y. Zhong, L. Zhang, and Y. Xu, "Spatial group sparsity regularized nonnegative matrix factorization for hyperspectral unmixing," *IEEE Trans. Geosci. Remote Sens.*, vol. 55, no. 11, pp. 6287–6304, 2017.

[7] W. He, H. Zhang, and L. Zhang, "Total variation regularized reweighted sparse nonnegative matrix factorization for hyperspectral unmixing," *IEEE Trans. Geosci. Remote Sens.*, vol. 55, no. 7, pp. 3909–3921, 2017.

[8] Y. Qian, S. Jia, J. Zhou, and A. Robles-Kelly, "Hyperspectral unmixing via $l_{1/2}$ sparsity-constrained nonnegative matrix factorization," *IEEE Trans. Geosci. Remote Sens.*, vol. 49, no. 11, pp. 4282–4297, 2011.

[9] S. Zhang, G. Zhang, F. Li, C. Deng, S. Wang, A. Plaza, and J. Li, "Spectral-spatial hyperspectral unmixing using nonnegative matrix factorization," *IEEE Trans. Geosci. Remote Sens.*, pp. 1–13, 2021.

[10] C. Févotte and J. Idier, "Algorithms for nonnegative matrix factorization with the β-divergence," *Neural computation*, vol. 23, no. 9, pp. 2421–2456, 2011.

[11] T. Ince and N. Dobigeon, "Weighted residual NMF with spatial regularization for hyperspectral unmixing," *IEEE Geosci. Remote Sens. Lett.*, vol. 19, pp. 1–5, 2022.

[12] J. M. Bioucas-Dias and M. A. T. Figueiredo, "Alternating direction algorithms for constrained sparse regression: Application to hyperspectral unmixing," in *Proc. 2nd Workshop Hyperspectral Image Signal Process., Evol. Remote Sens. (WHISPERS)*, June 2010, pp. 1–4.

[13] M. D. Iordache, J. M. Bioucas-Dias, and A. Plaza, "Collaborative sparse regression for hyperspectral unmixing," *IEEE Trans. Geosci. Remote Sens.*, vol. 52, no. 1, pp. 341–354, Jan 2014.

[14] ——, "Total variation spatial regularization for sparse hyperspectral unmixing," *IEEE Trans. Geosci. Remote Sens.*, vol. 50, no. 11, pp. 4484–4502, Nov 2012.

[15] R. Wang, H. Li, A. Pizurica, J. Li, A. Plaza, and W. J. Emery, "Hyperspectral unmixing using double reweighted sparse regression and total variation," *IEEE Geosci. Remote Sens. Lett.*, vol. 14, no. 7, pp. 1146–1150, July 2017.

[16] S. Zhang, J. Li, H. Li, C. Deng, and A. Plaza, "Spectral-spatial weighted sparse regression for hyperspectral image unmixing," *IEEE Trans. Geosci. Remote Sens.*, vol. 56, no. 6, pp. 3265–3276, June 2018.

[17] R. A. Borsoi, T. Imbiriba, J. C. M. Bermudez, and C. Richard, "A fast multiscale spatial regularization for sparse hyperspectral unmixing," *IEEE Geosci. Remote Sens. Lett.*, vol. 16, no. 4, pp. 598–602, 2019.

[18] T. Ince and N. Dobigeon, "Fast hyperspectral unmixing using a multiscale sparse regularization," *IEEE Geosci. Remote Sens. Lett.*, vol. 19, pp. 1–5, 2022.

[19] H. Li, R. Feng, L. Wang, Y. Zhong, and L. Zhang, "Superpixel-based reweighted low-rank and total variation sparse unmixing for hyperspectral remote sensing imagery," *IEEE Trans. Geosci. Remote Sens.*, pp. 1–19, 2020.

[20] T. Ince, "Superpixel-based graph Laplacian regularization for sparse hyperspectral unmixing," *IEEE Geosci. Remote Sens. Lett.*, pp. 1–5, 2020.

[21] ——, "Double spatial graph Laplacian regularization for sparse unmixing," *IEEE Geosci. Remote Sens. Lett.*, pp. 1–5, 2021.

[22] J. M. Bioucas-Dias, A. Plaza, N. Dobigeon, M. Parente, Q. Du, P. Gader, and J. Chanussot, "Hyperspectral unmixing overview: Geometrical, statistical, and sparse regression-based approaches," *IEEE J. Sel. Topics Appl. Earth Observ. Remote Sens.*, vol. 5, no. 2, pp. 354–379, April 2012.

[23] R. N. Clark *et al.*, *USGS digital spectral library splib06a*. U.S. Geological Survey Denver, CO, 2007.

[24] ——, "Imaging spectroscopy: Earth and planetary remote sensing with the USGS Tetracorder and expert systems," *J. Geophys. Res.*, vol. 108, no. E12, p. 5131, Dec. 2003.